SAND2022-13809C

SolarPACES 2022

Point Focus Systems

https://doi.or/10..... DOI placeholder (WILL BE FILLED IN BY TIB Open Publishing)

Published: (WILL BE FILLED IN BY TIB Open Publishing)

Design of a High Flux Beam Characterization Device for Falling Particle Receivers

Nathan Schroeder[1] and Braden Smith [2]

[1] R&D S&E Mechanical Engineer, Master of Science Mechanical Engineering. 1611 Innovation Pkwy NE, Albuquerque, NM 87123 United States of America, (505) 844-4945, nrschro@sandia.gov

[2] Sandia National Labs, (505) 844-8879, bsmith4@sandia.gov

Abstract. This paper outlines the design and error analysis for a flux characterization device (i.e. flux wand) which traverses the aperture of a falling particle receiver cavity providing the incident power measurement needed for the calculation of receiver efficiency without significantly disrupting receiver output. The design features a linear actuator, water cooled extension arm, and refractory bar. The refractory bar/flux wand is a diffusely reflective surface which reflects light as it is translated across the receiver aperture to provide a light intensity distribution that is correlated to a measured flux. The component sizing, constrained by a typical 30 frame per second camera and a 4-point average of the measured reflectance, is presented. Simulation reveals the error that results from a 5% variation in flux wand reflectance is within 4% of the true value.

Keywords: Falling Particle Receiver, Flux Characterization, G3P3

Introduction and Background

The Generation 3 Particle Pilot Plant (G3P3) currently under construction at the National Solar Thermal Test Facility (NSTTF) will be a fully integrated particle based concentrating solar power (CSP) system including a 2 MW falling particle receiver (FPR), hot bin with 6 hours of thermal energy storage, cold storage bin, particle to sCO_2 heat exchanger, 1 MW sCO_2 cooling loop, and particle lift. The goal of the project is to demonstrate the performance of each component within the system. The primary performance indicator for falling particle receiver subsystem is the thermal efficiency. The thermal efficiency is defined as the ratio of power absorbed by the particles and the power incident to the cavity receiver. In this paper, the design and uncertainty analysis of a non-disruptive method of measuring the power incident on the receiver cavity will be outlined.

Flux Wand Design

Measuring the power incident to the falling particle receiver requires the characterization of the flux distribution. Traditionally, the flux distribution is determined by positioning the beam on a diffuse reflecting water cooled calibration panel, measuring the intensity of the reflected light, and correlating that intensity with a measured flux value with a beam characterization system (BCS) [1]. Avoiding disruption to the power delivered to the G3P3 system is critical for continuous operation, therefore the beam cannot be moved from the receiver cavity for characterization. Instead, a thin linear actuated diffuse surface (also known as a “Flux Wand”) traverses the receiver aperture providing a reference surface that is used to characterize the flux distribution within the receiver. The flux wand will be paired with a separate flux

measurement device that is inserted and retracted from the cavity to provide a correlation between the intensity of reflected light and solar flux.

Many flux measurement techniques, including the flux wand, were outline by Röger et al [2]. The design which utilizes the beam characterization system (BCS) developed by Sandia in the later 1970's [1] was down selected from options such as an array of flux gauges on a moving bar [3] or an indirect measurement of light from the receiver which utilizes DNI measurements, a recorded image of the sun, and the receiver reflectivity [4]. The simplicity of the flux wand design together with the relatively low expected error were the main reasons for its consideration.

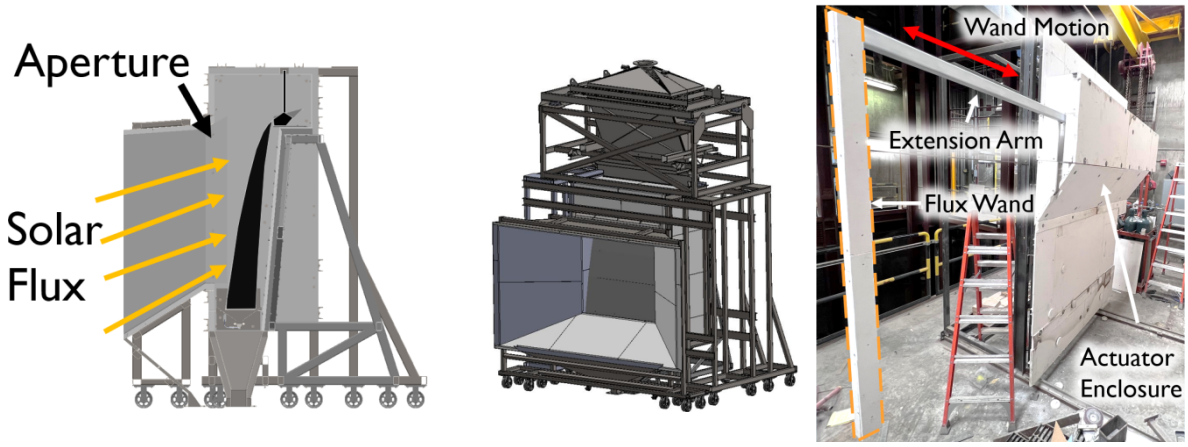

(a) (b) (c)

Figure 1. G3P3 2 MW_{th} receiver cavity in a side (a) and isometric view (b) and flux wand test stand with component labels (c)

The flux wand is composed of a stainless-steel Unistrut channel support member, an attached section of high temperature, diffuse, refractory reflective material (RSLE-57), a water/air cooled extension arm, and a 2 meter throw linear actuator, which is shown in Figure 1. The flux gauge (Hukseflux GG01-1000) is mounted to a pneumatic actuator to extend into and retract out of the receiver, not shown. During operation, the flux wand traverses the receiver cavity at the aperture plane while a camera records reflected solar energy from the surface. Following the transit, the flux gauge extends to provide a correlating flux value. In post processing, the image frames containing the flux wand, recorded by the camera, are stitched together to form a continuous pixel intensity distribution. The intensity of the pixels that fall within the measurement aperture of the flux gauge are then correlated to the measured flux value. This intensity/flux calibration is used to convert the remaining pixel intensity values to flux using a linear correlation. Finally, the spatial flux values are summed to determine the total power incident to the receiver cavity.

Aperture Flux Reconstruction

Wand Motion Simulation

A frame simulator developed in Python was used to help estimate the accuracy of the stitching algorithm. Simulated frames of the flux wand translating across the receiver aperture are generated. The simulator has full control over physical parameters of the simulation, such as the wand transition speed and width, camera frame rate, and flux distribution. This simulator includes estimates of image blurring, shot noise, and camera noise that are expected to be observed during experimentation. Required inputs to the simulation are illustrated in Figure 2.

Applying our reconstruction algorithm to simulated frames is an important step in estimating the uncertainty in this measurement device. It would be much more difficult to estimate the accuracy using only the assembled flux wand setup due to uncontrolled variables such as unknown wand soiling and real flux distribution. Additionally, simulated frames allow us to test the reconstruction algorithm under best-case conditions as well as anticipated soiled conditions. This not only gives confidence that the reconstruction algorithm will work when the hardware is in new condition, but that it will continue to provide accurate results after extended use of the equipment and aging/soiling becomes more present.

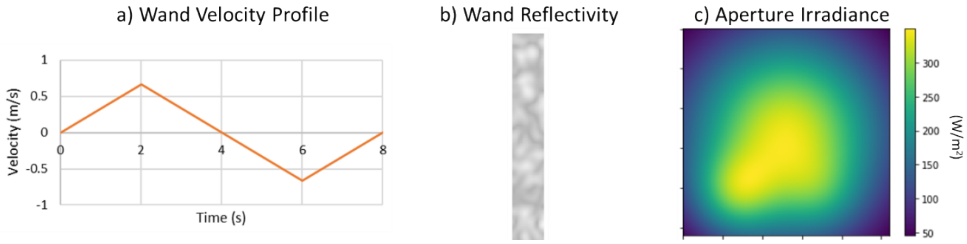

Figure 2. Inputs into flux wand simulation: a) flux wand translation velocity profile, b) flux wand reflectivity map ranging from 85% to 90%, and c) simulated aperture irradiance distribution created by summing 2D Gaussian functions.

Aperture Flux Reconstruction Algorithm

The reconstruction algorithm was tested on simulated frames. For each frame, the algorithm locates the edges of the wand and identifies the active region of the image. Since the simulated incident flux is exactly known, the accuracy of the algorithm can be directly calculated for various degrees of wand soiling.

The edges of the wand are found using a method similar to that used by Ferriere et al. [5], and is illustrated in Figure 3. The pixel intensity of the image is summed in the vertical direction of the Example Frame in Figure 3, and then the first and second derivatives are calculated. The first derivative is used to identify the right and left edges of the wand and the second derivative is used to calculate the extent of the edge blur of the wand. The wand edges are found for every frame of the video and stitched together, averaging pixel data when multiple frames contain the wand surface. The irradiance image will be radiometrically calibrated using the flux gauge measurement inside the aperture.

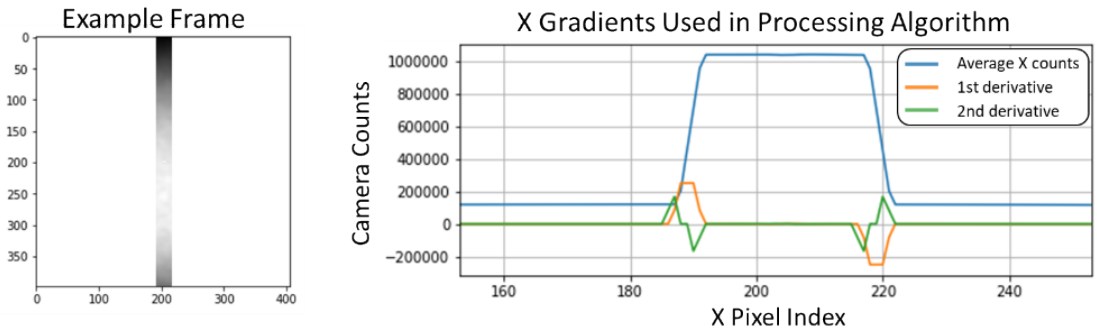

Figure 3. Example flux wand frame with calculated image gradients

Results

Component Sizing

The camera, linear actuator, and flux gauge have been specified for the G3P3 receiver. The minimum wand width that would not leave any uncaptured areas of the aperture between camera frames, given a camera frame rate of 30Hz, is shown as a function of wand transition time in Figure 4. A wider wand and/or slower transition time can allow for multiple point averages of the entire aperture area, at the cost of blocking more solar flux incident on the G3P3 receiver. Wand sizes that allow up to four-point averages are targeted for the wand size and transition time. A 5 cm wand size was selected which imposes a 3.5 second transition time to provide the four-point average. Multiple point averages will help mitigate wand surface reflection irregularities and unavoidable noise in the imaging system.

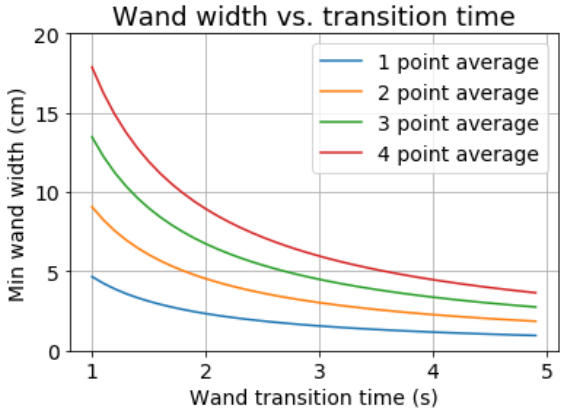

Figure 4. Flux wand width vs receiver transition time

Image Processing

The image processing software was tested on simulated frames of the wand translating across a 132cm aperture. Flux wand reflectance values ranging from 85% to 90% were imposed to simulate anticipated soiling. Figure 5 shows the results of the simulation. The left image shows the normalized synthetic irradiance profile, the center image shows the normalized irradiance profile generated by the image processing software, and the right image shows the expected error with this configuration. Variations in the wand's reflectance can be seen in the "streaking" visible in the rightmost image. Error in the individual pixel irradiance values is expected to be up to 4% when using a soiled wand.

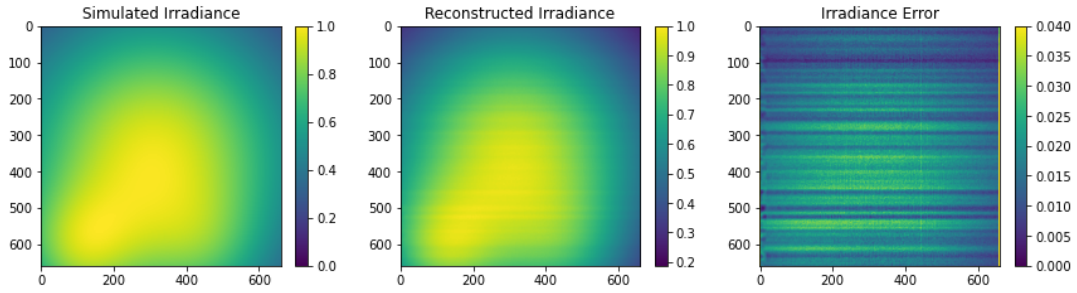

Figure 5. From left to right: synthetic irradiance profile, reconstructed irradiance profile generated from the simulated wand translation, and expected error.

Test Setup

An at-scale demonstration of the flux wand including the flux wand mechanical system, shown in Figure 1 (c), and the image processing software will be conducted at the existing Sandia National Laboratories' National Solar Thermal Test Facility (NSTTF) tower. This test will 1) determine the temperature rise of the RSLE and cooling fluid within the extension arm during a transit through flux levels similar to what is expected in the G3P3 FPR, 2) demonstrate the use of the image processing software, and 3) provide confidence in the consistent operation of the linear actuator. Given the successful demonstration of the flux wand within the current tower, the current G3P3 receiver design will be modified to implement this system.

Conclusion

The design of a flux characterization device, i.e. flux wand, which characterizes the flux distribution incident to a cavity receiver via a moving reflective surface was presented. The system operates by recording images of the surface as it transitions in front of the receiver and stitching the images containing the wand together to form a continuous intensity distribution of the light reflected from the surface. The width of the flux wand and transition time was determined by imposing a four-point average for each pixel given a 30 Hz frame rate camera. A 5 cm wand was fabricated, and the linear actuator was programed for a 3.5 second transition time. The system was simulated in Python to provide estimation of the error due to wand soiling. With a variable reflectance between 85-90% a 4% error is expected.

Author contributions

Nathan Schroeder: Conceptualization, Methodology, Project Administration, Writing Original Draft

Braden Smith: Data Curation, Formal Analysis, Software, Visualization, Writing Original Draft

Competing interests

The authors declare no competing interests.

Funding

Please insert funding statement (if applicable) here.

Acknowledgement

This work was funded in part or whole by the U.S. Department of Energy Solar Energy Technologies Office under Award Number DE-EE0008730. This report was prepared as an account of work sponsored by an agency of the United States Government. Neither the United States Government nor any agency thereof, nor any of their employees, makes any warranty, express or implied, or assumes any legal liability or responsibility for the accuracy, completeness, or usefulness of any information, apparatus, product, or process disclosed, or represents that its use would not infringe privately owned rights. References herein to any specific commercial product, process, or service by trade name, trademark, manufacturer, or otherwise does not necessarily constitute or imply its endorsement, recommendation, or favoring by the United States Government or any agency thereof. The views and opinions of the authors expressed herein do not necessarily state or reflect those of the United States Government or any agency thereof.

Sandia National Laboratories is a multimission laboratory managed and operated by National Technology and Engineering Solutions of Sandia, LLC., a wholly-owned subsidiary of Honeywell International, Inc., for the U.S. Department of Energy's National Nuclear Security Administration under contract DE-NA0003525.

References

[1] E. Thalhammer, "Heliostat Beam Characterization System—Update," presented at the ISA-79 National Conference adn Exhibit, Chicago, Illinois, 1979.

[2] M. Roger, P. Herrmann, S. Ulmer, M. Ebert, C. Prahl, and F. Gohring, "Techniques to Measure Solar Flux Density Distribution on Large-Scale Receivers," *Journal of Solar Energy Engineering,* vol. 136, 2014.

[3] J. Pacheco, R. Houser, and A. Neumann, "Hybrid Heat Flux Measurement System for Solar Central Receiver Evaluation " *Energy,* vol. 29, pp. 917-924, 2004.

[4] C. K. Ho and S. S. Khalsa, "A Photographic Flux Mapping Method for Concentrating Solar Collectors and Receivers," (in English), *J Sol Energ-T Asme,* vol. 134, no. 4, Nov 2012, doi: Artn 041004

Doi 10.1115/1.4006892.

[5] A. Ferriere, M. Volut, A. Perez, and Y. Volut, "In-situ measurement of concentrated solar flux and distribution at the aperture of a central solar receiver," presented at the AIP Conference Proceedings, 2016. [Online]. Available: https://doi.org/10.1063/1.4949217.